Supporting Information

Dipole-dipole Interactions for Inhibiting Solvent Co-intercalation into Graphite Anode to Extend the Horizon of Electrolyte Design

Mingsheng Qin,[a] [b] Ziqi Zeng,*[a] Qiang Wu,[a] Hui, Yan,[c] Mengchuang, Liu,[a] Yuanke Wu,[a] [b] Han Zhang,[a] Sheng, Lei,[a] Shijie Cheng[a] and Jia Xie*[a]

[a]State Key Laboratory of Advanced Electromagnetic Engineering and Technology, School of Electrical and Electronic Engineering, Huazhong University of Science and Technology, Wuhan 430074, P. R. China.

[b]State Key Laboratory of Materials Processing and Die & Mould Technology, School of Materials Science and Engineering, Huazhong University of Science and Technology, Wuhan 430074, P. R. China

[c]Institute of Metal Research, Chinese Academy of Sciences, Shenyang 110000, P. R. China

*Correspondence: xiejia@hust.edu.cn (J. Xie), ziqizeng@hust.edu.cn (Z. Zeng)

Experiments and Methods

Materials.

Propylene carbonate (PC, 99%), diethyl carbonate (DEC, 99%), were purchased from Guangzhou Tinci Materials Technology Co., Ltd. 1,2-dimethoxyethane (DME, 99.5%), trimethyl phosphate (TMP, 99%), dimethyl sulfoxide (DMSO, 99%) dimethyl carbonate (DMC), ethylene carbonate (EC) and ethyl methyl carbonate (EMC) were obtained from Sigma-Aldrich. lithium bis(fluorosulfonyl)imide (LiFSI, 99.5%) was purchased from Dodo Chem, Suzhou, China. Carboxymethyl cellulose (CMC) was purchased from Daicel Chemical Industries Ltd. Japan. Li foil (φ 14 mm, 200 μm, China Energy Lithium Co., Ltd.), Cu foil (12 μm, Shenzhen Kejing Star Technology Co., Ltd.) and separator (Celgard 2400) were also employed for cell assembly. All of these chemicals were employed without other purifications,

Electrolyte and electrode preparations.

All electrolytes were prepared based on the molar ratios. For example, The LiFSI-3DME-7FB was prepared by dissolving one molar LiFSI in three molar DME solution, forming a transparent and clear solution. 7 molar FB was added into above solution to get the wanted electrolyte. The same procedure was carried for other electrolytes. Note that negligible DEC was introduced into BB-PC and CB-PC mixed solutions to get miscible solutions, which will not destruct the solvation structure and molecular interactions model for the negligible contents and much lower binding energy of Li-DEC pairs. The graphite electrodes were prepared by mixing graphite, CMC and Super P with a mass ratio of 8:1:1. The formed slurry was coated on Cu foil and heated at 80 ^{o}C for two days. The average active mass loading was 1.5~2 mg cm^{-2}. The graphite//Li cells were assembled with graphite electrodes and Li metal foil with a constant electrolyte of 40 μL if not specified. The practical $LiFePO_4$//graphite pouch cells were supplied by EVE Energy Co., Ltd. Note that 2wt% FEC was added to stabilize $LiFePO_4$ lattice and inhibit possible electrode crosstalk in pouch cells.

Electrochemical measurements and characterizations.

The graphite//Li cells were measured on battery testing system (Neware battery test system, CT-4008T-5V50Ma-164). Electrochemical impedance spectrometry (EIS) (100 kHz to 0.1 Hz) was carried out on Solartron electrochemical workstation with voltage amplitude of 10 mV, Cyclic voltammetry (CV) were measured by a CHI 600D

at a scan rate of 0.1 mV s^{-1}. In situ XRD signals were collected by the VANTEC-500 detector in a still mode based on the special battery model. Raman spectroscopy was collected by LabRAM HR800 (HORIBA Jobin Yvon IBH Ltd.) with 785 nm laser. NMR results were collected on Ascend 600 MHz (Bruker. Co., Ltd.). Specifically, the 1 M LiCl in deuterated water was sealed in quartz capillary for internal standard. The sealed quartz capillary and electrolyte were put into the NMR tube to collect ^{7}Li signals. electrolytes and separators were employed to measure contact angle at KRUSS DSA100.

Theoretical calculations

Quantum Chemistry Calculations: The Density Functional Theory (DFT) calculation were performed in ORCA program. The geometrical structures were calculated at B3LYP-GD3BJ/6-311G** level. The calculations in FB solvation were carried out with the implicit universal solvation model based on Conductor-like Continuum Polarization Model (C-PCM). The binding energy (E_b) between Li^+ and solvate molecules was defined as following:

$$E_b = E_{total} - E_{Li+} - E_{sol}$$

where E_{total}, E_{Li+}, and E_{sol} are the total energy of the Li^+-solvate complexes, Li^+, and solvate molecules, respectively.

Ab-Initial Calculations: The calculation related to the interaction between solvate molecules and graphite was conducted by using the CP2K package. The Perdew-Burke-Ernzerhof (PBE) exchange correlation functional at DZVP-MOLOPT-SR-GTH basis set were used to describe the system. A plane-wave energy cut-off and relative cut-off of 400 Ry and 55 Ry have been employed, respectively. The SCF convergence criterion was set to 10^{-6} Hartree. The Grimme's empirical DFT-D3 was used to describe the van der Waals (vdW) interactions between slab and molecular. A 6×6 graphite (001) slab with a 20 Å vacuum space was used to represent the absorbed surface. The absorbed energy between graphite (001) slab and different solvate molecules was defined as following equation:

$$E_a = E_{slab+mol} - E_{slab} - E_{mol}$$

where $E_{slab+mol}$, E_{slab} and E_{mol} are the energy of the complex, graphite slab, and solvate molecules, respectively.

Molecular Dynamics (MD) Simulations: The classical MD simulations were performed by using the GROMACS package. The forced field parameters were obtained from GROMOS96 54a7 force field. Four different solutions systems consisting of 50 Li-FSI/150 DME, 50 Li-FSI/150 DME/350 FB, 50 Li-FSI/250 DME and 50 Li-FSI/250 DME/350 FB were simulated in different periodic boundary conditions boxes. The electrostatic interactions were treated using the Particle-Mesh-Ewald (PME) methods. A cutoff length of 1.0 nm was used in the calculation of electrostatic interactions and non-electrostatic interactions in real space. The integration time step was 1 fs. To make the initial configurations more reasonable, the structural optimization was conducted firstly. For equilibrium processes, the temperature and pressure coupling were performed in V-rescale and Berendsen method, respectively. The systems were annealed from 0 to 298 K over a period of 0.5 ns, following by running for another 2.0 ns to reach equilibrium. For production simulations, the pressure coupling method in production simulation period was changed to Parrinello-Rahman. Production simulation ran 100 ns for post-processing analysis.

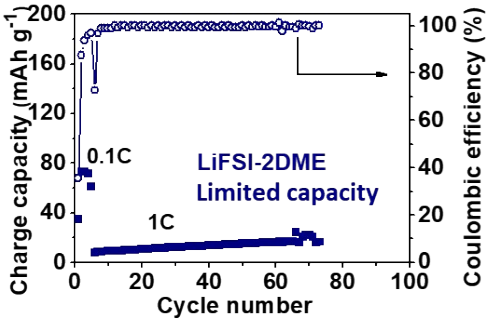

Figure S1. The cycling performance of graphite//Li cell in LiFSI-2DME.

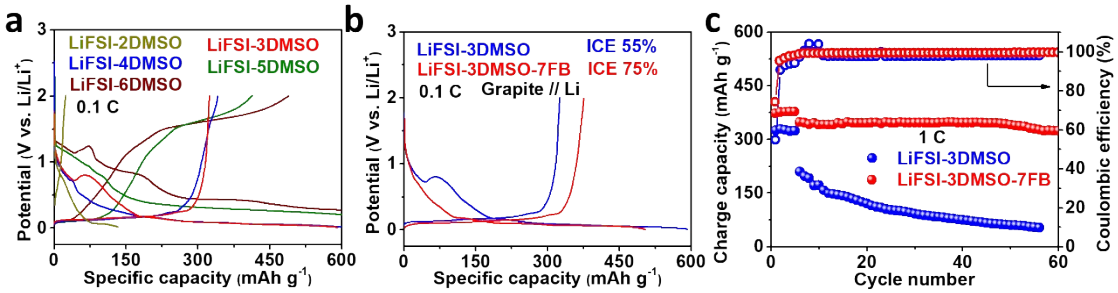

Figure S2. Rational design of electrolyte with DMSO. The charge-discharge curves of (a) LiFSI/DMSO with different MRs and (b) LiFSI-3DMSO and LiFSI-3DMSO-7FB. (c) The cycling stability of graphite//Li cells in LiFSI-3DMSO and LiFSI-3DMESO-7FB electrolyte. The LiFSI-3DMSO is defined as the critical MR since severe cointercalation at lower MRs and large polarization at higher MRs. Graphite exhibits cointercalation plateau at 0.8 V in LiFSI-3DMSO but represents reversible intercalation in LiFSI-3DME-7FB. The fast capacity fading during cycling also indicates the graphite-incompatibility of LiFSI-3DMSO electrolyte.

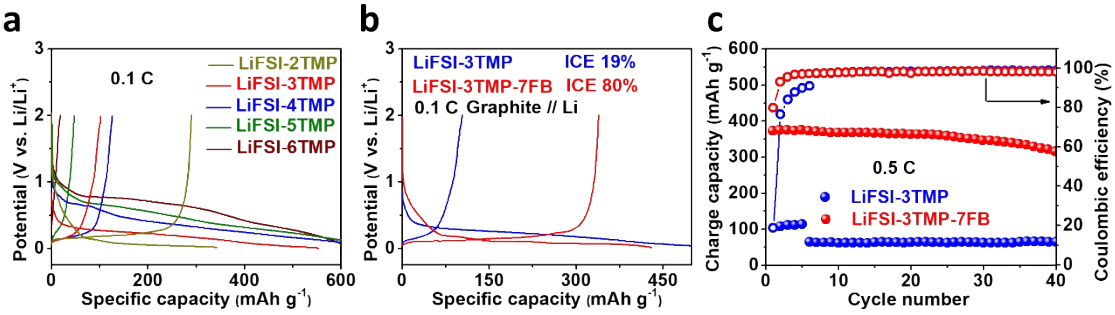

Figure S3. Rational design of electrolyte with TMP. The charge-discharge curves of (a) LiFSI/TMP with different MRs and (b) LiFSI-3TMP and LiFSI-3TMP-7FB. (c) The cycling stability of graphite//Li cells in LiFSI-3TMP and LiFSI-3TMP-7FB electrolyte. Graphite can cycle reversibly in LiFSI-2TMP but suffers from long discharging plateau with low ICE of 19% in LiFSI-3TMP. Moreover, a limited capacity below 100 mAh g^{-1} is obtained in LiFSI-3TMP. As the result, the LiFSI-3TMP is defined as the critical MR. The introduction of FB enhances the ICE and sustains reversible cycling.

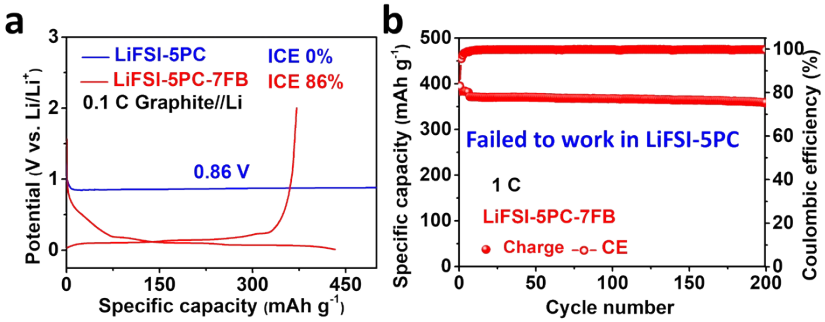

Figure S4. Rational design of electrolyte with PC. The charge-discharge curves of (a) LiFSI-5PC and LiFSI-5PC-7FB. (b) The cycling stability of graphite//Li cells in LiFSI-5PC and LiFSI-5PC-7FB electrolyte. Graphite exhibits endless Li^+-PC cointercalation at 0.86 V in LiFSI-5PC and the LiFSI-5PC is defined as critical MR. The reversible cycling and high ICE can be obtained once adding FB into LiFSI-5PC.

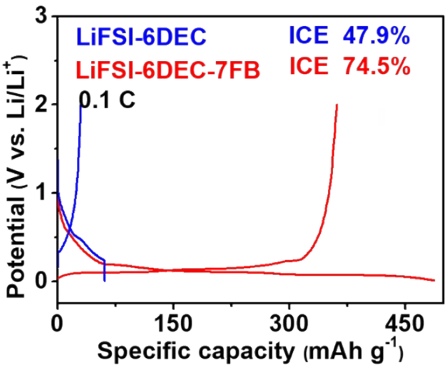

Figure S5. The charge-discharge curves of LiFSI-6DEC and LiFSI-6DEC-7FB.

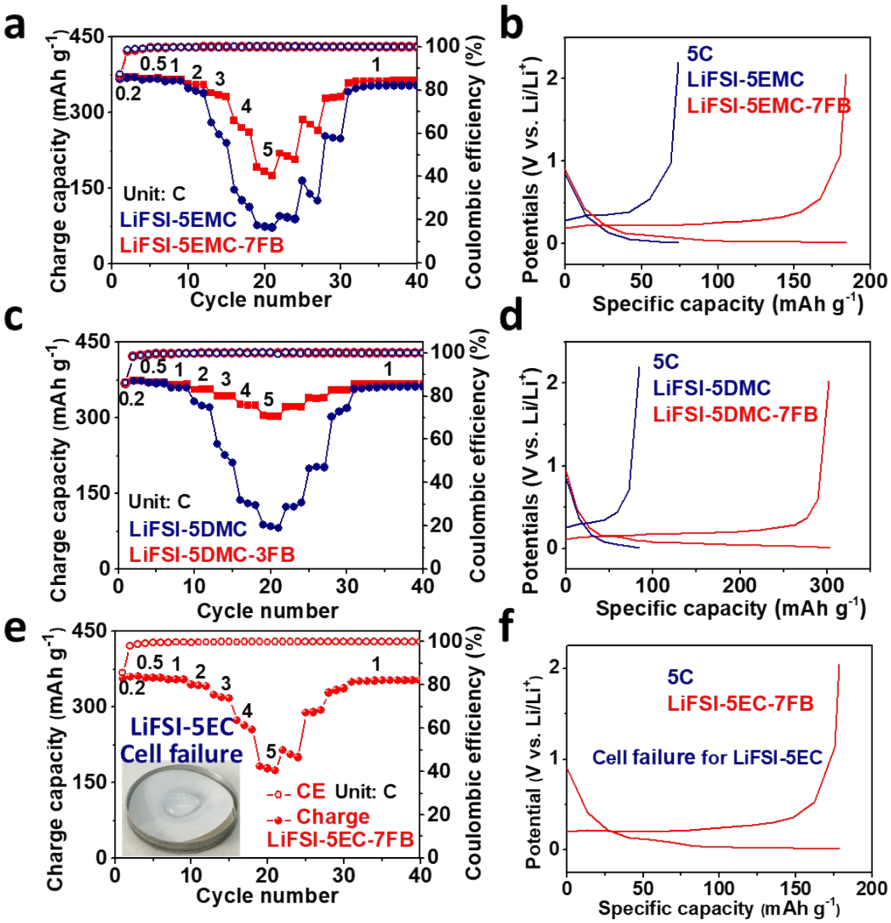

Figure S6. The rate performances of graphite//Li cells in (a-b) EMC-based, (c-d) DMC-based and (e-f) EC-based electrolytes. The adding of FB results in better rate capabilities for all graphite-compatible electrolytes (EMC, DMC and EC). Note that graphite//Li cell falls into cell failure in LiFSI-5EC as denoted by the poor wettability on PP separator. The improved rate performance is caused by: 1) FB decreases viscosity and promotes good wettability towards separator. 2) The dipole-dipole interaction among FB and solvents (e.g., EMC, DMC and EC) facilitates desolvation and interfacial reaction.

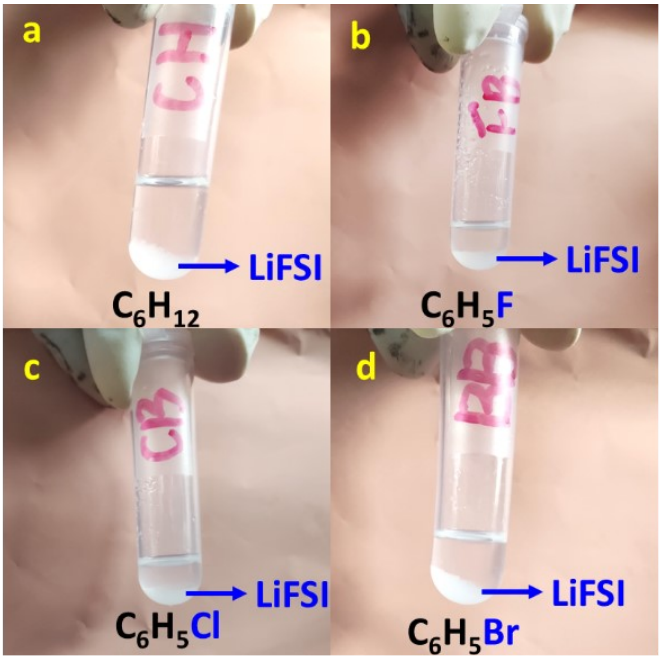

Figure S7. The pictures of LiFSI dissolved in (a) cyclohexane, (b) fluorobenzene, (c) chlorobenzene and (d) bromobenzene. The precipitation at the bottom indicates the negligible solubility of LiFSI in these solvents. For this reason, the C_6H_{12}, C_6H_5F, C_6H_5Cl and C_6H_5Br are defined as non-solvents.

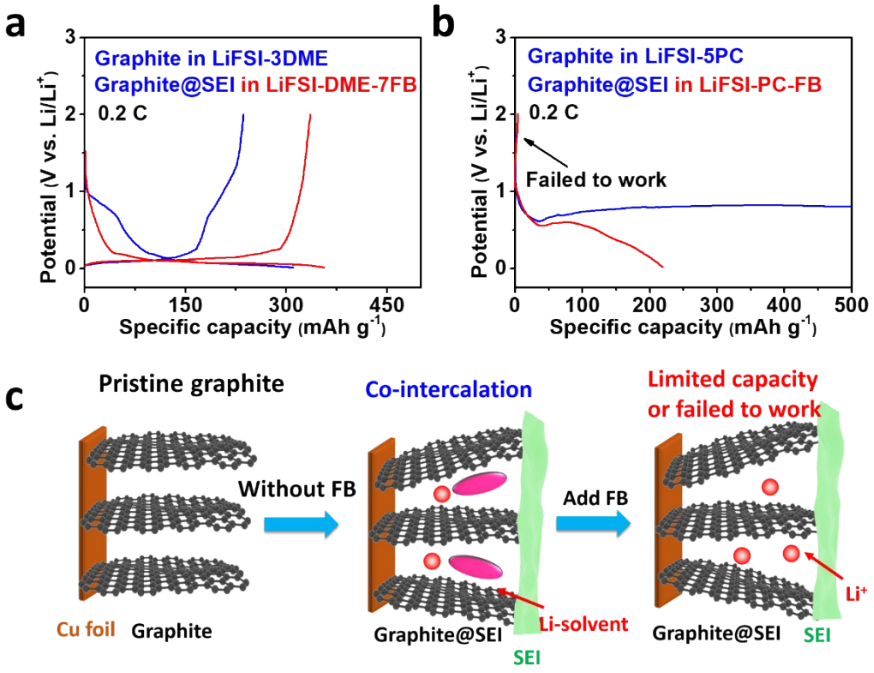

Figure S8. SEI validation in varied electrolytes. (a) Graphite cycled in LiFSI-3DME is reassembled in LiFSI-3DME-7FB. (b) Graphite cycled in LiFSI-5PC is reassembled in LiFSI-5PC-7FB. (c) Illustrations for the limited effects of SEI for inhibiting co-intercalation. Note that the co-intercalation of Li^+-DME clusters proves reversible at some extent and damage graphite structure partially. Therefore, the graphite cycled in LiFSI-3DME can still exhibit reversible capacity of 330 mAh g^{-1} after reassembling. The gap between theoretical and practical capacity is caused by the partially destructed graphite structure. The graphite discharged in LiFSI-5PC, by contrast, cannot work after reassembled with LiFSI-5PC-7FB due to the completely destructed structure in LiFSI-5PC. As a result, the poor SEI coated graphite (cycled in LiFSI-3DME) can cycle normally in LiFSI-3DME-7FB, further demonstrating the dominant roles of bulk electrolyte than SEI for inhibiting co-intercalation.

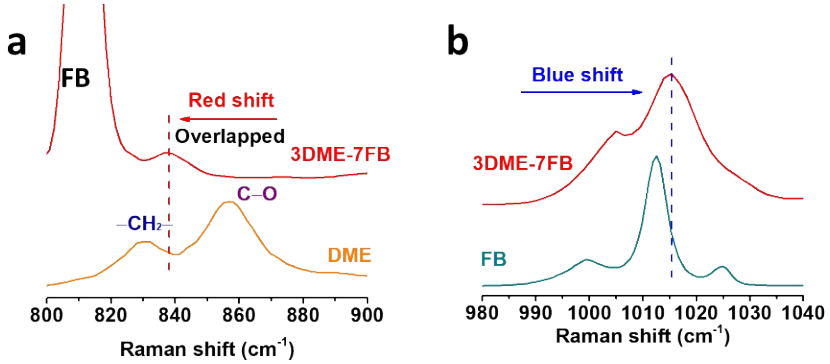

Figure S9. The Raman results of (a) DME and DME-FB mixed solution, (b) FB and DME-FB mixed solution. The CH_2 rocking modes and C–O stretching bands of DME are overlapped upon FB addition, with significant red shift, demonstrating the molecular interactions between FB and DME. Similarly, the blue shift is observed for the mixing of C–O stretching and C–H in-plane bending modes for FB.

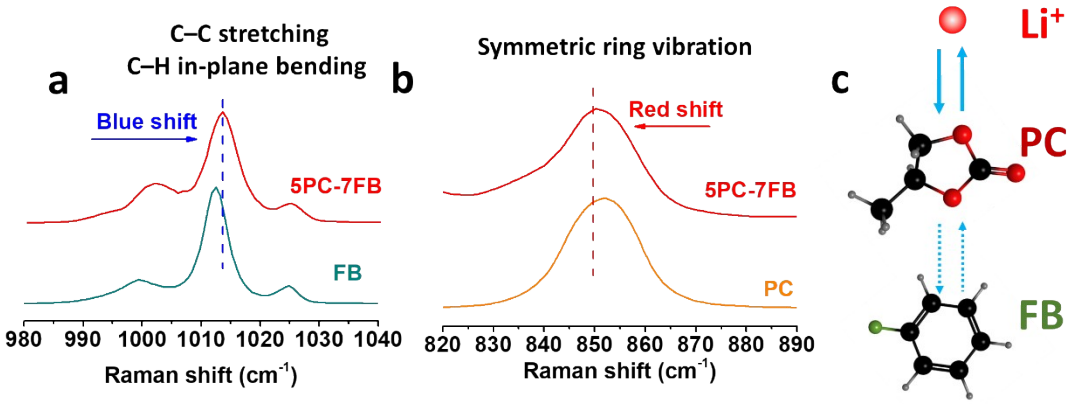

Figure S10. The molecular interactions between FB and PC solvents. The Raman results of (a) FB and PC-FB mixed solution, (b) PC and PC-FB mixed solution. (c) Schematic illustrations for the interactions of Li^+, PC and DME. Note that the overlap of C–C stretching and C–H in-plane bending modes in FB involves blue shift after PC addition. Moreover, the symmetric ring vibrations of PC exhibits red shift, corresponding to the FB results. These interplays can be illustrated in Figure S10c, in which Li^+ exerts strong Coulombic attractions to PC while FB represents molecular interactions to PC, forming the competition model.

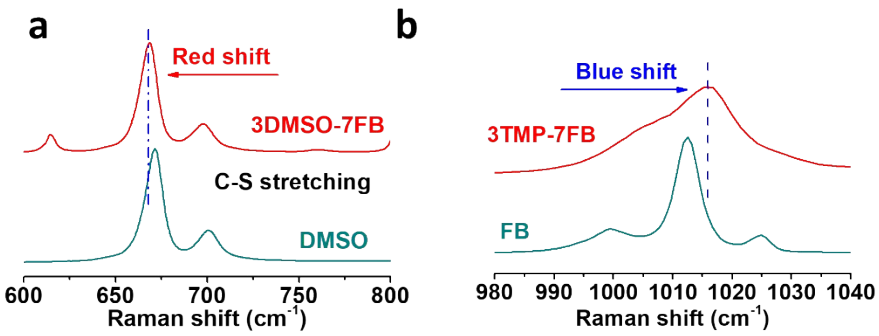

Figure S11. (a) The Raman shift of C-S stretching for DMSO after FB addition. (b) The Raman shift of FB in 3TMP-7FB. The blue shift upon blending FB with solvents (e.g., DMSO and TMP) indicates the molecular interaction between solvents and non-solvents.

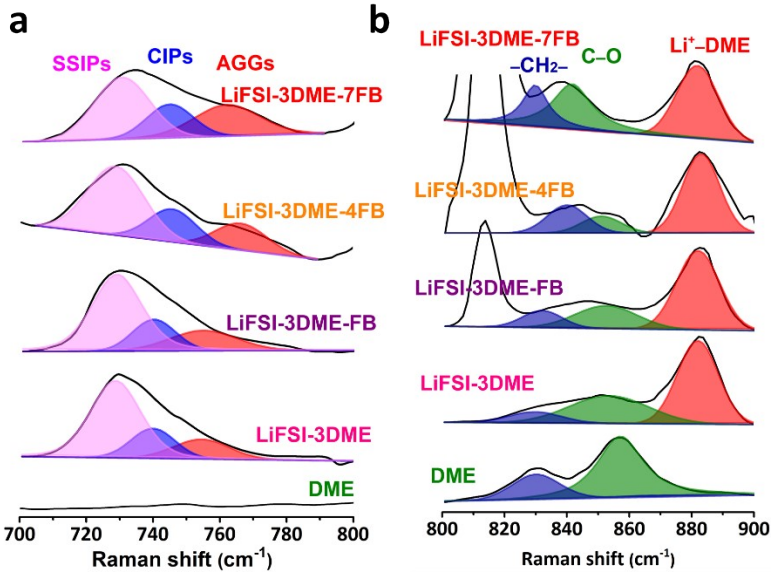

Figure S12. The Rama spectra of (a) S-N-S bending motions for FSI^- anions and (b) for DME solvents in different electrolytes

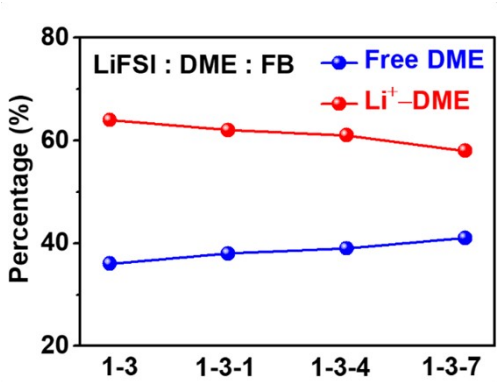

Figure S13. The negligible increase of free DME molecules upon FB addition.

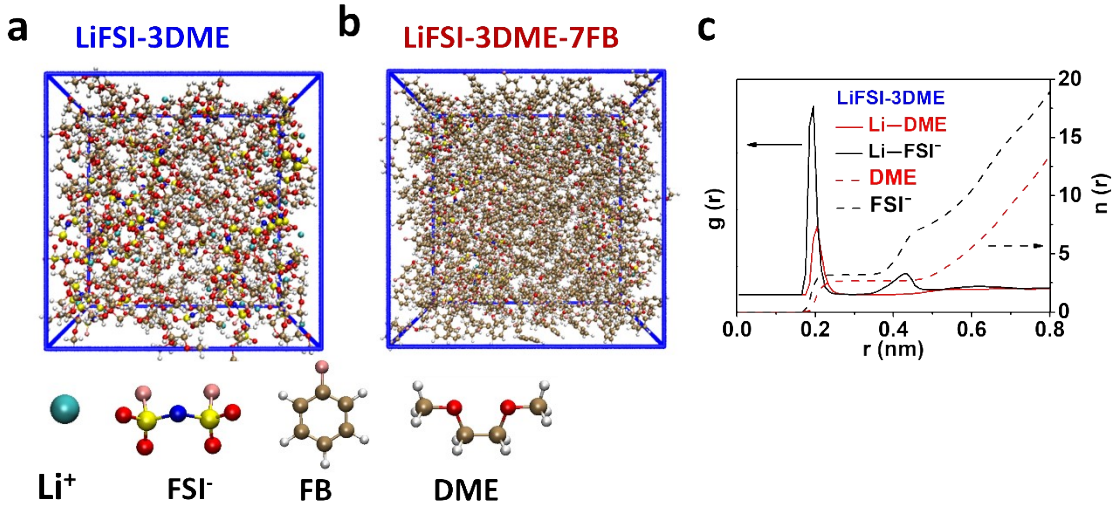

Figure S14. MD studies of the Li^+ solvation structure. Snapshot of the MD simulation cell for the (a) LiFSI-3DME and (b) LiFSI-3DME-7FB. (c) RDFs of Li^+-(O)DME and Li^+-(O)FSI^- in LiFSI-3DME.

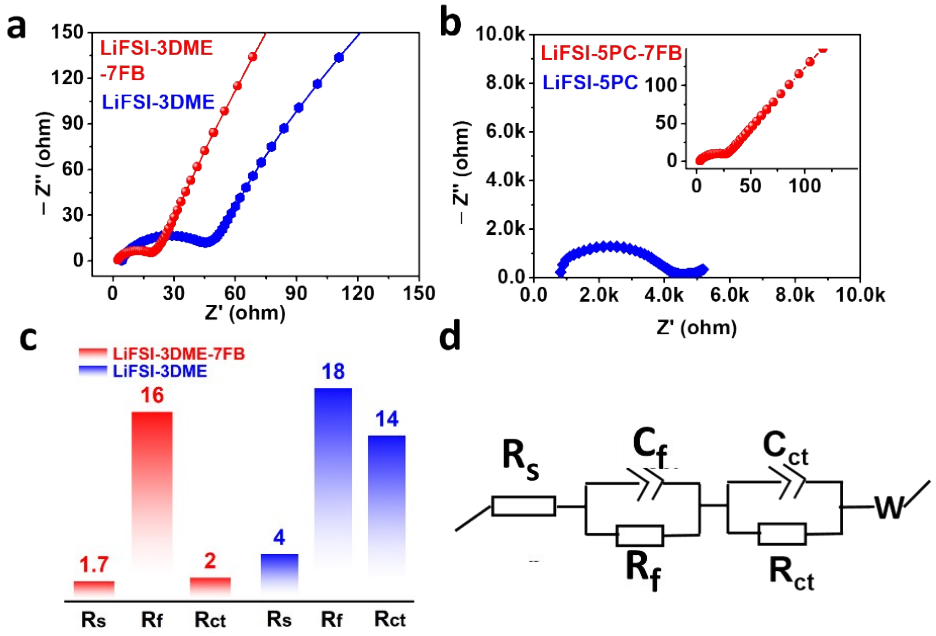

Figure S15. Electrochemical impedance spectra for graphite/Li cells in (a) LiFSI-3DME and LiFSI-3DME-7FB, (b) LiFSI-5PC and LiFSI-5PC-7FB after initial cycle. (c) The simulated R_s (bulk resistance), R_f (SEI resistance) and R_{ct} (charge-transfer resistance) from corresponding EIS results. (d) The fitting circuit.

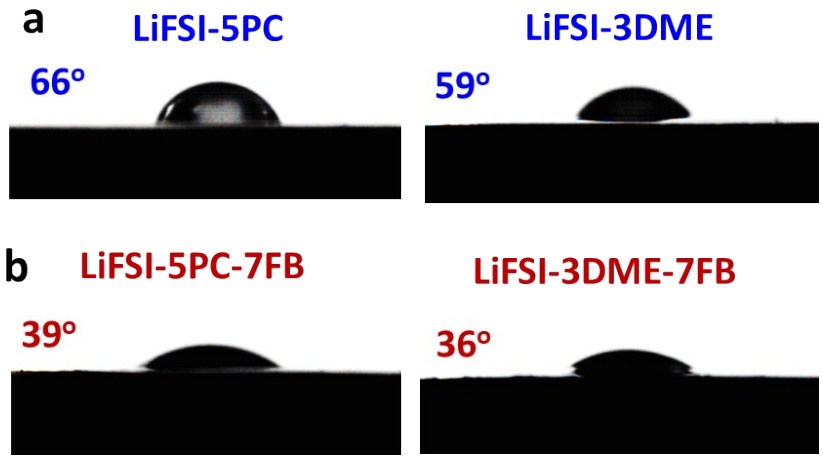

Figure S16. The wettability tests of the separator contact with (a) LiFSI-5PC and LiFSI-3DME, (b) LiFSI-5PC-7FB and LiFSI-3DME-7FB.

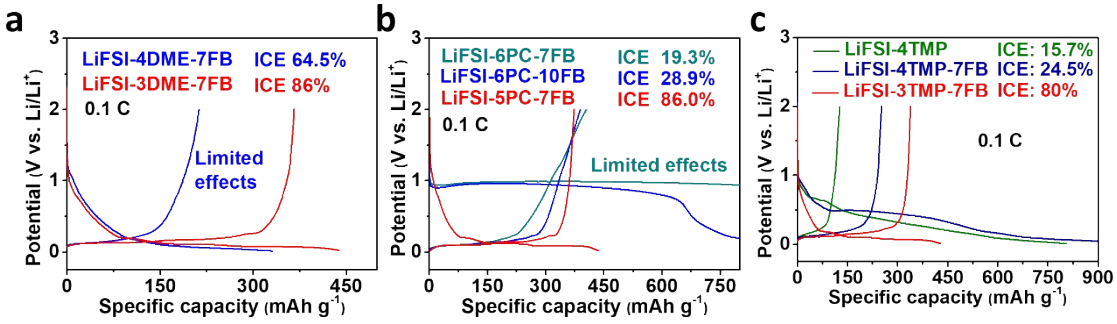

Figure S17. The initial charge-discharge curves for graphite//Li cells with different electrolytes. (a) LiFSI-4DME-7FB and LiFSI-3DME-7FB. (b) LiFSI-6PC-7FB, LiFSI-6PC-10FB and LiFSI-5PC-7FB. (c) LiFSI-4TMP, LiFSI-4TMP-7FB and LiFSI-3TMP-7FB. The critical LiFSI/DME MR proves to be 1:3 since the failure of LiFSI-4DME-7FB. Similarly, the critical LiFSI/PC MR is 1:5 and LiFSI/TMP MR is 1:3. The addition of FB below critical MRs exhibits inferior ICEs, indicating the limited effects of solvents-nonsolvents interactions in this scenario. The LiFSI-6PC-10FB exhibits slightly increased ICE compared to LiFSI-6PC-7FB, but still far from the LiFSI-5PC-7FB, further indicating the significance of critical Li salts/Solvent MRs for effectiveness of nonsolvents-solvents interactions.

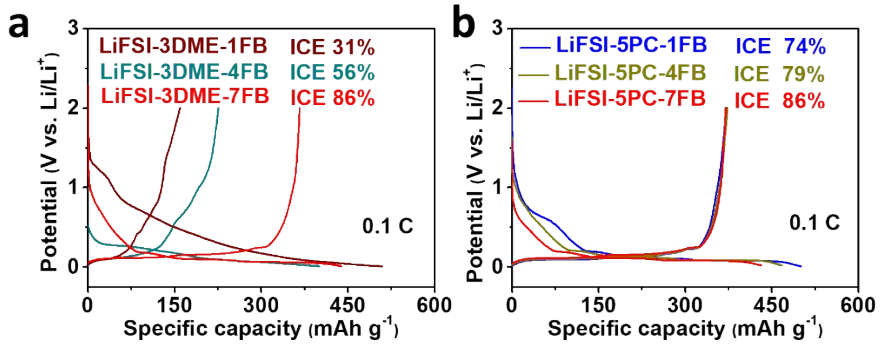

Figure S18. The initial charge-discharge curves for graphite/Li cells in (a) DME-based electrolyte with varied FB contents and (b) PC-based electrolyte with varied FB contents. the nonsolvents-solvents interactions increase with adding more FB, leading to increased ICE accordingly.

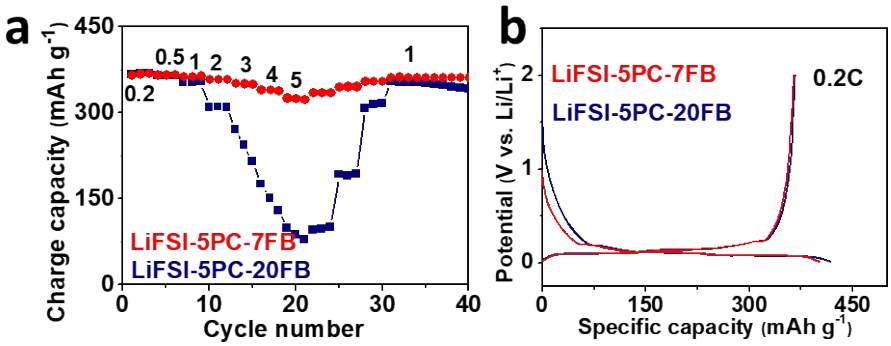

Figure S19. The rate performance of graphite//Li cells upon further increasing FB. The LiFSI-5PC-7FB affords decent rate capability with 323 mAh g^{-1} even at 5C, indicating the beneficial effects of dipole-dipole interaction for expediting electrochemical kinetics. However, excessive FB leads to diluted Li salts concentration and inferior rate performance, highlighting the importance of rational electrolyte design.

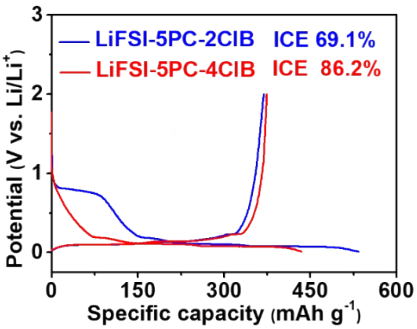

Figure S20. The initial charge-discharge curves for graphite//Li cells in PC-based electrolyte with different ClB contents. Graphite//Li cells can be operated normally in LiFSI-5PC-4ClB while failed in LiFSI-5PC-2ClB, indicating the desirable ClB contents of four molars.

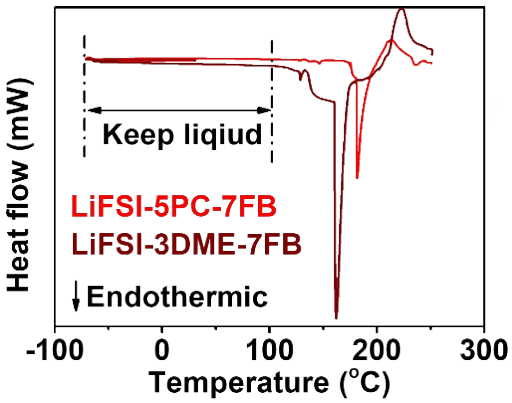

Figure S21. DSC results of PC-based and DME-based electrolytes.

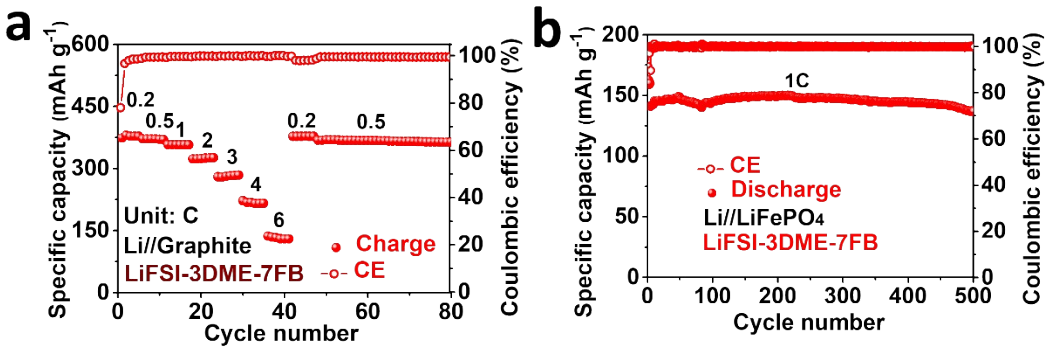

Figure S22. The (a) rate capability of graphite//Li cell and (b) cycling stability of Li//$LiFePO_4$ cell in LiFSI-3DME-7FB electrolyte.

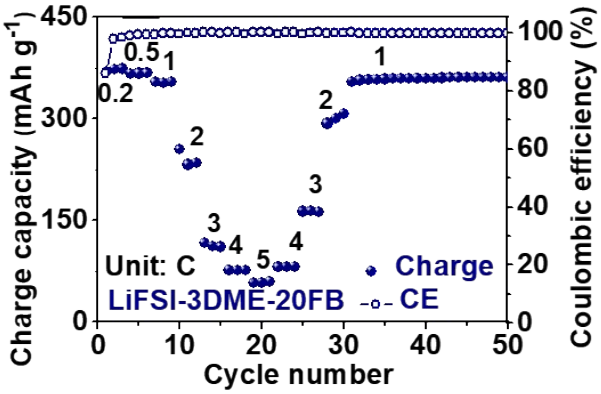

Figure S23. The rate capability of graphite//Li cell in LiFSI-3DME-20FB.

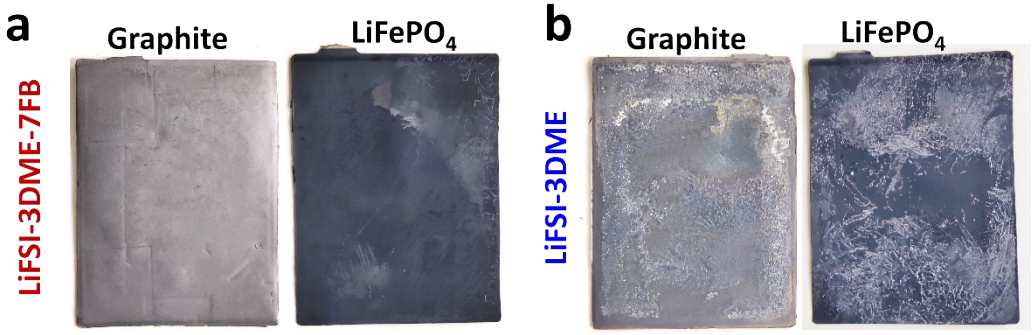

Figure S24. The pictures of $LiFePO_4$ and graphite electrodes disassembled from pouch cells filled with varied electrolytes.

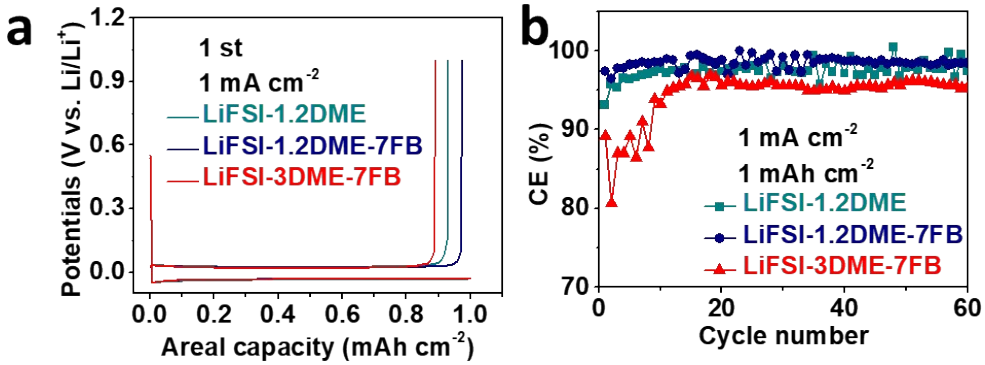

Figure S25. The performance of Li//Cu cells. (a) Initial deposition-stripping curves and (b) CEs of Li//Cu cells in different electrolytes. The LiFSI-1.2DME-7FB exhibits superior reversibility than LiFSI-1.2DME, which is caused by the low viscosity and possible fluorination from FB. In contrast, LiFSI-3DME-7FB shows inferior performance since abundant free DME within bulk electrolyte.

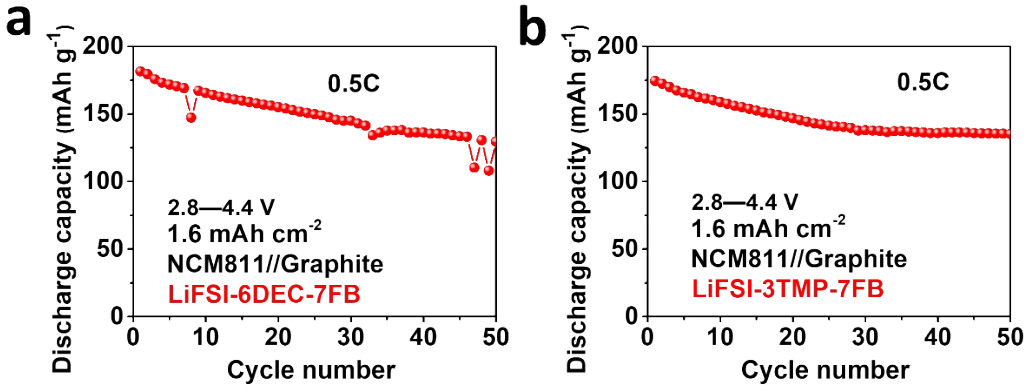

Figure S26. The cycling stabilities of NCM811//graphite cells in (a) LiFSI-6DEC-7FB and (b) LiFSI-3TMP-7FB electrolytes. All graphite-incompatible solvents are capable of working in LIBs with the help of FB non-solvents, which weakens Li^+-solvent strength and thus facilitate desolvation near graphite surface. Note that these electrolytes are just as prototypes without optimizing other parts. The much improved long-term cycling stability can be obtained after introducing additives, advanced Li salts and electrode optimizations.